crystals

MDPI

Article

On the Size Effect of Strain Rate Sensitivity and Activation Volume for Face-Centered Cubic Materials: A Scaling Law

Xiazi Xiao [1], Hao Liu [2] and Long Yu [3,*]

[1] Department of Mechanics, School of Civil Engineering, Central South University, Changsha 410075, China; xxz2017@csu.edu.cn

[2] Department of Applied Physics, School of Physics and Electronics, Hunan University, Changsha 410082, China; haoliu@hnu.edu.cn

[3] State Key Laboratory for Turbulence and Complex System, Department of Mechanics and Engineering Science, College of Engineering, Peking University, Beijing 100871, China

* Correspondence: yulong123@pku.edu.cn; Tel.: +86-13126976377

Received: 7 September 2020; Accepted: 2 October 2020; Published: 3 October 2020

Abstract: In a recent experimental study of indentation creep, the strain rate sensitivity (SRS) and activation volume v^* have been noticed to be dependent on the indentation depth or loading force for face-centered cubic materials. Although several possible interpretations have been proposed, the fundamental mechanism is still not well addressed. In this work, a scaling law is proposed for the indentation depth or loading force-dependent SRS. Moreover, v^* is indicated to scale with hardness H by the relation $\partial \ln(v^*/b^3)/\partial \ln H = -2$ with the Burgers vector b. We show that this size effect of SRS and activation volume can mainly be ascribed to the evolution of geometrically necessary dislocations during the creep process. By comparing the theoretical results with different sets of reported experimental data, the proposed law is verified and a good agreement is achieved.

Keywords: indentation creep; size effect; strain rate sensitivity; activation volume; geometrically necessary dislocations

1. Introduction

Over recent decades, instrumented indentation tests have been recognized as an effective tool for probing the thermally activated deformation of metallic materials [1–3]. Typical experimental methods for the study of indentation creep contain the constant load and hold (CLH) test [4], constant strain rate (CSR) test [5], constant loading rate (CLR) test [6], strain rate jump (SRJ) test [7], etc. Being different from the conventional creep tests, the strain rate sensitivity (SRS) and activation volume (the two critical rate sensitive parameters) measured by these creep tests have been noticed to exhibit an obvious size effect [2,7–9]. The comprehension of these size-dependent parameters is critically essential for the interpretation of the fundamental creep deformation mechanisms [1,10–12].

So far, there exist two types of size effect as informed from the tests of indentation creep, including the interface-dominant creep size effect [7,9,11,13–16] and indentation depth- or force-related creep size effect [2,8,17–23]. For the former, previous literature has indicated that both the SRS and activation volume are affected by the intrinsic microstructures like grain and twin boundaries at the micro- or nano-scale [24,25]. For face-centered cubic (FCC) materials, enhanced SRS with decreasing grain size has been observed for nanocrystalline gold [14], copper [13] and nickel [11]. As for nano-twinned materials, a similar scaling relation has also been noticed for the dependence of SRS on the twin thickness [26,27]. It is, therefore, realized that there exists an intrinsic length scale for the SRS and activation volume, which is determined by the grain size and twin width of nanostructured materials [7,9,11,13–15] or the

film thickness of nanocrystalline films [28–30]. In order to interpret the thermally activated mechanisms for this length scale, Asaro and Suresh [26] proposed an analytical model by considering the emission of partial dislocations from grain and twin boundaries. Following this idea, a non-homogeneous nucleation model was later developed that can rationalize the size-dependent SRS and activation volume for nanocrystals and nano-twinned materials [31].

Besides the influence of intrinsic microstructures, there exists another form of size effect when addressing the indentation creep of single crystals and polycrystals with large grain size, i.e., the SRS decreases or the activation volume increases with increasing indentation depth or loading force, and this phenomenon has been widely observed in the CLH [19,21,22,32,33], CSR [8,23,34,35] and SRJ [36–38] test. For example, the size effect of indentation creep has been studied for polycrystalline pure aluminum through CLH tests at room temperature, which exhibits an obvious decreasing tendency of the SRS with increasing loading force even after the correction of thermal drift effects [22]. Similarly, the SRS of both annealed and 80% cold-worked 70/30 brass has been noticed to decrease with increasing indentation depth when performed under CSR tests [35]. Moreover, when applying SRJ tests on sintered silver nanoparticles, the SRS decreases from 0.04 to 0.024 with the increase in indentation depth from 1100 nm to 1700 nm [37]. Therefore, it is anticipated that there exist some different mechanisms for the depth- or force-related creep size effect of single or polycrystals, when compared with the interface-dominant creep size effect of nanocrystals or nano-twinned polycrystals.

In recent years, several possible explanations have been proposed for addressing the depth- or force-related creep size effect, including the consideration of the free surface effect [21], thermal drift [2,19] and the evolution of geometrically necessary dislocations (GNDs) [2,8,39,40]. Sadeghilaridjani et al. [21] attribute this creep size effect to the high diffusion and mobility of dislocations near the sample surface, which result in a comparatively high SRS at shallow indents. However, even when the indentation depth extends 100 nm so that the influence of the free surface can be ignored, the size effect can still be observed in brass [35] and Al alloys [23]. Another possible explanation is considered to be the influence of thermal drift [2,19]. It is believed that the measurement error could exceed 100% when the indentation displacement rate gets close to the thermal drift rate [2]. However, even if the thermal drift is artificially inhibited or corrected during the indentation creep tests, the creep size effect still exists, especially at shallow indentation depths [23]. Actually, it is interesting to note that the depth- or force-related creep size effect seems to follow a similar evolution tendency as the hardness–force (or depth) relation of polycrystalline aluminum and alpha brass [8]. For the latter, it is with the well-known indentation size effect that the hardness decreases with increasing indentation depth due to the influence of GNDs [41]. Consequently, the fundamental mechanisms addressing the creep size effect are believed to originate from the thermally activated interaction between GNDs, which could become comparatively difficult as the density of GNDs becomes high at shallow indents [8,39,40].

In this work, we intend to propose a mechanistic model scaling the depth- or loading force-dependent SRS and activation volume of FCC materials, as corresponding theoretical analyses addressing this creep size effect have been seldomly reported in the literature. The outline of this paper is given as follows: in Section 2, the theoretical model is proposed in detail for the creep size effect. In Section 3, the experimental data of alpha brass, aluminum and austenitic steel are considered to verify the rationality and accuracy of the model results. Finally, we close with a brief conclusion in Section 4.

2. Theoretical Model for the Creep Size Effect

To begin with, the creep process under indentation tests is considered to be accommodated with the evolution of dislocation microstructures beneath the indenter tip. At the onset of creep deformation, dislocation loops with Burgers vectors normal to the surface plane are generated to address the geometrical shape change at the contact surface [41]. Then, the existing GNDs are forced to move radially from the inner creep region (close to the indenter tip) to the boundary between the creep and

elastic regions. For simplicity, we assume that the creep deformation can be discretized into numbers of sequential activation events. During each activation event, the indenter tip moves downwards by a distance of b, and forces the i-th dislocation loop ($1 \le i \le N$ with N being the number of dislocation loops) to sweep a distance of s. Here, b is the magnitude of the Burgers vector and s is the spacing between dislocation loops [41], as illustrated in Figure 1.

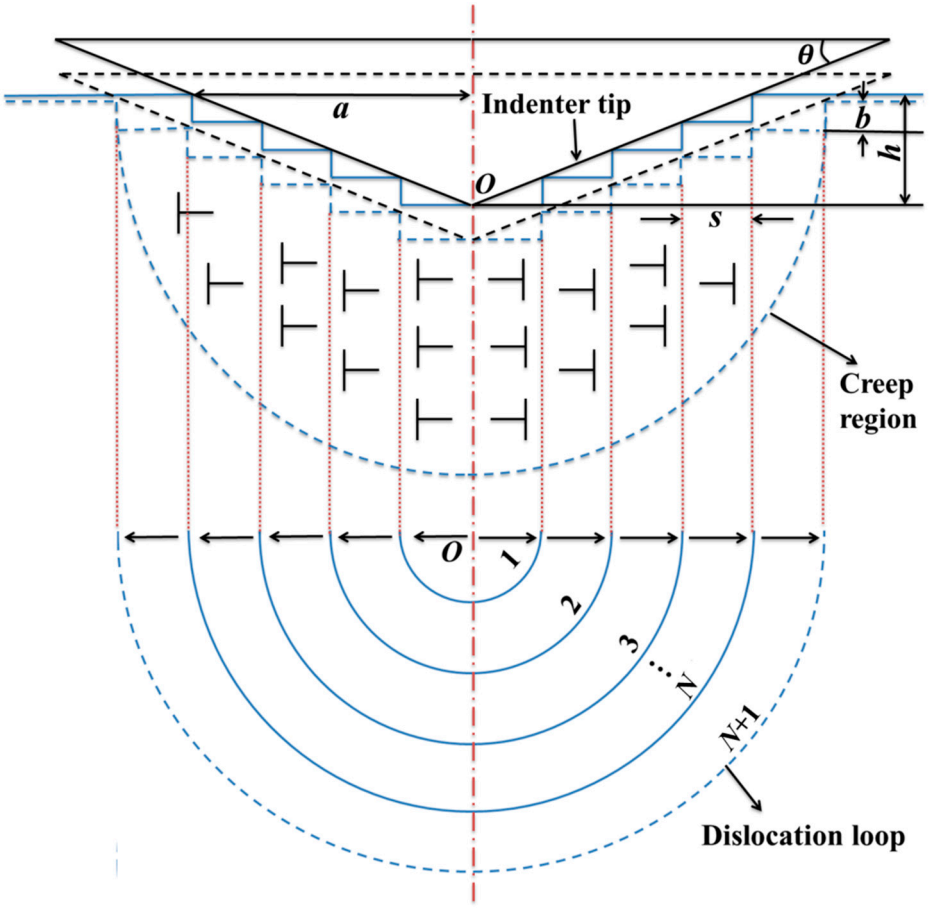

Figure 1. Schematic of indentation creep with the evolution of geometrically necessary dislocations (GNDs), which are performed by a conical indentation. When $\tan\theta = \sqrt{\pi/24.5} = 0.358$ (θ is the angle between the indenter and sample), the model is also applicable to the Berkovich indentation following the self-similar principle [41]. The creep process is discretized into the expansion of circular dislocation loops. During each creep activation, the indenter tip moves forward by a length of b, and a new dislocation loop is generated from the indenter tip that forces existing dislocation loops to creep radially with a distance of s. Thereinto, b and s are, respectively, the magnitude of the Burgers vector and the spacing between individual dislocation loops.

2.1. Size Effect of the Activation Volume

Considering that the total length of GNDs is $\lambda = \pi ha/b$ [41] and the number of dislocation loops equals $N = h/b$, the average length of the dislocation segment within the creep region yields

$$l_G^* = \frac{\lambda}{N} = \pi a = \pi h \cot\theta \tag{1}$$

where a and h are, respectively, the contact radius and indentation depth. θ is the angle between the indenter and sample. In addition, the activation distance between each dislocation loop becomes

$$d_G^* = s = \frac{ba}{h} \tag{2}$$

When one further considers the obstacle-determined dislocation plasticity [24,42], the activation volume determined by GNDs can then be expressed as

$$v_G^* = bl_G^* d_G^* = \pi b^2 \cot^2\theta h = \frac{3\pi b}{2}\frac{1}{\rho_G} \tag{3}$$

where $\rho_G = 3\tan^2\theta/(2bh)$ is the depth-dependent GND density, as defined by Nix and Gao [41]. Equation (3) indicates that v_G^* increases proportionally with h but varies inversely with ρ_G. A similar evolution tendency has already been observed for swaged and annealed copper where the activation volume increases almost linearly with h [18]. Given that the activation distance is a constant, as indicated by Equation (2), the variation of v_G^* is then realized to be determined by the evolution of l_G^*.

As the creep process goes on, the density of GNDs gradually decreases due to the expansion of the creep region with increasing indentation depth. Although the transition of pre-existing statistically stored dislocations (SSDs) to GNDs might be possible by the cross-slip mechanism [43], its influence on the decrease in GND density may not be obvious, as the dominant type of dislocation is the edge dislocation for FCC materials considered in this work. Then, the thermal activation of SSDs tends to dominate the creep deformation. For crystalline materials with large grain size, the average segment length and activation distance of SSDs can be, respectively, estimated as $l_S^* \sim k/\sqrt{\rho_S}$ and $d_S^* \sim 1/\sqrt{\rho_S}$ with ρ_S being the density of SSDs [24]. Then, to be consistent with Equation (3), the activation volume related to SSDs could be taken as

$$v_S^* = bl_S^* d_S^* = \frac{3\pi b}{2}\frac{1}{\rho_S} \tag{4}$$

where $\rho_S = 3\tan^2\theta/(2bh^*)$ and $k = 3\pi/2$. Thereinto, h^* is a characteristic length related to the bulk hardness [41]. It is indicated by Equation (4) that v_S^* is independent of h but characterizes the intrinsic creeping properties of materials without size effect.

When simultaneously addressing the contribution of GNDs and SSDs, one may consider the relation $1/v^* = 1/v_G^* + 1/v_S^*$ [27], and then the general expression of the activation volume yields

$$v^* = \frac{3\pi b}{2}\frac{1}{\rho_S + \rho_G} \tag{5}$$

which can be reduced to Equation (3) when there exists an obvious indentation size effect (i.e., $\rho_G >> \rho_S$), or be degraded into Equation (4) when $\rho_G \to 0$ at deep indents. Given the expressions of ρ_G and ρ_S as mentioned above, the activation volume can be recast as

$$v^* = \frac{\pi b^2 h^* H_0^2}{\tan^2\theta}\frac{1}{H^2} \tag{6}$$

and

$$\ln\left(\frac{v^*}{b^3}\right) = \ln k_2 - 2\ln H \tag{7}$$

where $H = H_0\sqrt{1 + h^*/h}$ is the depth-dependent indentation hardness [41], and $k_2 = \pi h^* H_0^2/(b\tan^2\theta)$ is a constant related to the bulk hardness H_0 and characteristic length h^* [44]. As indicated by Equation (7), $\ln(v^*/b^3)$ scales linearly with $\ln H$, which is consistent with the experimental observations for most FCC materials, like aluminum, silver and nickel [40]. In addition, the decrease in v^* with increasing H can be ascribed to the accumulation of dislocations at shallow indents that leads to a small activation area swept out by gliding dislocations during the thermal activation event [30].

2.2. Size Effect of the Strain Rate Sensitivity

Next, following the Taylor relation, the shear strength of FCC materials is determined by the dislocation density, i.e.,

$$\tau = \mu b\alpha\sqrt{\rho_S + \rho_G} \tag{8}$$

where μ is the shear modulus and α is the dislocation strength coefficient. The lattice friction τ_0 is ignored in the expression of τ as it is usually very small for FCC materials [45]. By further considering the von Mises flow rule [46] and Tabor's factor [47], the hardness can be given as

$$H = 3\sqrt{3}\tau = 3\sqrt{3}\mu b\alpha\sqrt{\rho_S + \rho_G} \tag{9}$$

Submitting Equations (5) and (9) into the definition of SRS, it yields

$$m = \frac{3\sqrt{3}k_BT}{v^*H} = \frac{2k_BT}{3\pi\mu\alpha b^2}\sqrt{\rho_S + \rho_G} \tag{10}$$

where k_B and T are the Boltzmann constant and testing temperature, respectively. Recalling the expressions of ρ_S and ρ_G as mentioned above, one can further have

$$m = \frac{2k_BT}{3\pi\mu\alpha b^2}\sqrt{\frac{3\tan^2\theta}{2bh^*} + \frac{3\tan^2\theta}{2bh}} = m_0\sqrt{1 + \frac{h^*}{h}} \tag{11}$$

where $m_0 = k_BT\tan\theta/(\pi\mu\alpha b^2)\sqrt{2/(3bh^*)}$ is the SRS without size effect for bulk materials that depends on the density of SSDs through h^*. Equations (10) and (11) indicate that both GNDs and SSDs contribute to the SRS measured by indentation creep tests. However, the variation of SRS with respect to the indentation depth is determined by the contribution of GNDs.

When one further takes the relation between the loading force P and h^2 in a proportional form [48], i.e., $P = Kh^2$ and $P^* = K(h^*)^2$, where K is a proportionality factor and P^* is the characteristic loading force corresponding to h^*, then the expression of Equation (11) can be recast as

$$m = m_0\sqrt{1 + \sqrt{\frac{P^*}{P}}} \tag{12}$$

It is interesting to note that Equations (11) and (12) offer a characteristic form for the depth dependence or loading force dependence of the SRS so that the square of the SRS scales linearly with the reciprocal of the indentation depth or of the square root of the loading force. When the raw experimental data of polycrystals are drawn in this way, a straight line is anticipated so that the intercept informs the value of m_0 and the slope yields h^* or P^*. In order to verify this proposed scaling law, four different sets of experimental data are considered in the following, including annealed and work-hardened alpha brass [8,49], annealed aluminum [8] under CLH tests, austenitic steel [38] under SRJ tests and annealed alpha brass [35] under CSR tests.

3. Comparison between Theoretical Results and Experimental Data

We firstly present the $m - P$ relationships of work-hardened mechanically polished alpha brass [49] and annealed aluminum [8], which are compared between the experimental data (black dots) and theoretical results (red lines), as illustrated in Figure 2. The creep tests are performed at room temperature with the loading force ranging from 10^{-4} to 10^0 N, and the type of indenter is a Berkovich indenter [8,49]. The theoretical results are predicted by Equation (12) with m_0 and P^* calibrated by comparison with the converted experimental data (see the inset of Figure 2). The model parameters are listed in Table 1. An excellent agreement is observed where the SRS decreases with the increase in P until m_0 is reached. This decreasing tendency is ascribed to the variation of creep mechanisms, which range from the dislocation–dislocation interaction to the dislocation–solute interaction, as the former becomes dominant at a high stress level [50]. Moreover, the fitted values of m_0, i.e., 0.016 and 0.007, for alpha brass and aluminum are, respectively, close to the literature values of 0.018 obtained by CSR tests for copper [19] and 0.01 obtained by CLH tests for aluminum [40].

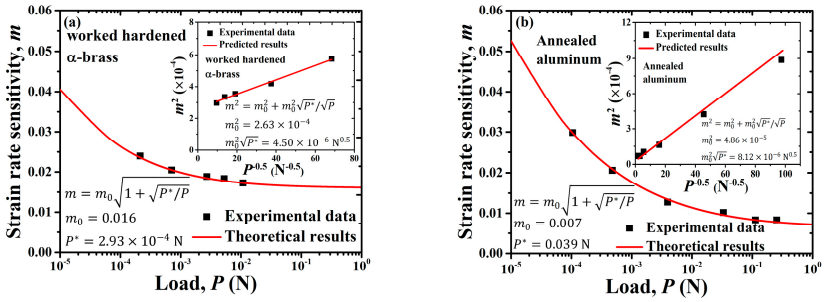

(**a**) (**b**)

Figure 2. Strain rate sensitivity m-loading force P relationships compared between the experimental data (black dots) and theoretical results (red lines) of (**a**) work-hardened mechanically polished alpha brass [49] and (**b**) annealed aluminum [8]. The inset figure illustrates the calibration of model parameters by comparison with experimental data.

Table 1. Model parameters for work-hardened alpha brass [49], annealed aluminum [8], austenitic steels [38] and annealed alpha brass [35].

Parameter	Work-Hardened Alpha Brass	Annealed Aluminum	Parameter	Austenitic Steels	Annealed Alpha Brass
m_0	0.016	0.007	m_0	0.006	0.0023
P^* (N)	2.94×10^{-4}	0.039	h^* (nm)	2023	6097

The proposed $m - P$ relation can also be expressed in a similar form as the classic Nix–Gao model [41] so that the SRS decreases with increasing indentation depth. In order to verify the $m - h$ relation, as indicated by Equation (8), the experimental data of austenitic steel (SRJ test) [38] and annealed alpha brass (CSR test) [35] are considered. A Berkovich indenter is applied for these creep tests. In Figure 3, the comparison between theoretical results and experimental data is illustrated so that a reasonable agreement is observed for both materials. In this case, $m_0 = 0.006$ for austenitic steel is close to 0.0066 for 310 stainless steel [51] and $m_0 = 0.0023$ matches well with 0.002 obtained from [49] for annealed alpha brass. However, one may note that the experimentally measured value of m for the alpha brass gradually deviates from the theoretically predicted line. This is believed to originate from the effect of thermal drift during the indentation creep tests. According to the analysis of [2], the SRS without thermal drift correction $\overline{m}$ can be approximated as $\overline{m} \equiv m(1 + \lambda/\dot{h})^2$ with λ as the thermal drift rate (of the order of $\pm 10^{-2}$ nm·s^{-1}) and $\dot{h}$ as the penetration rate. With increasing indentation depth, $\dot{h}$ decreases from an initial high value down to the absolute value of λ. Therefore, it is rational to observe that $\overline{m} < m$ with the increase in h when $\lambda < 0$, as indicated in Figure 3b.

Besides the characteristic $m - h$ and $m - P$ relationships as proposed above, the normalized activation volume with respect to the indentation hardness also follows a scaling law, as expressed in Equation (7). To verify this conclusion, the experimental data of copper obtained from [30,52], as well as the data of alpha brass and aluminum taken from [8], are plotted in Figure 4. Correspondingly, the scaling relation is illustrated by solid lines with the slope $\partial \ln(v^*/b^3)/\partial \ln H = -2$. It seems that the creep data follow this scaling law well, and similar linear relationships between $\ln(v^*/b^3)$ and $\ln H$ have also been noticed in the experimental data of some other FCC materials, but with the slope ranging from −1 to −3 [40]. This discrepancy may originate from ignoring the effect of strain hardening induced by the dislocation–dislocation interaction, and might also come from the influence induced by thermal drift through $v^* = k_B T/(m\tau)$, as the simulation work of [19] has captured an obvious variation of SRS with increasing thermal drift rate.

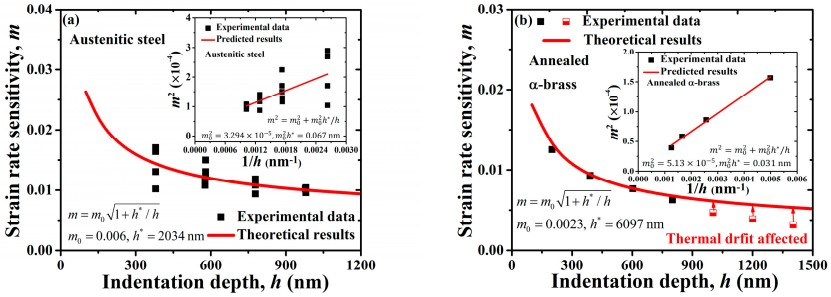

(**a**) (**b**)

Figure 3. Strain rate sensitivity m-indentation depth h relationships compared between the experimental data (black dots) and theoretical results (red lines) of (**a**) austenitic steel [38] and (**b**) annealed alpha brass [35]. The inset figure illustrates the calibration of model parameters by comparison with experimental data.

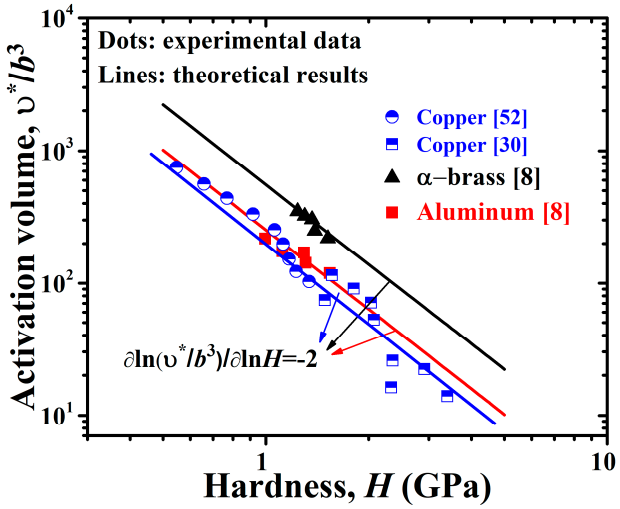

Figure 4. Normalized activation volume v^*/b^3–hardness H relationships compared between experimental data (dots) and theoretical results (lines) for copper [30,52], alpha brass [8] and aluminum [8].

4. Conclusions

To sum up, a scaling law is proposed in this work to address the indentation depth- or loading force-dependent SRS for FCC materials, i.e., $m = m_0\sqrt{1+h^*/h}$ or $m = m_0\sqrt{1+\sqrt{P^*/P}}$. In addition, the activation volume is found to scale with the hardness by the relation $\partial \ln(v^*/b^3)/\partial \ln H = -2$. The model is deduced by the consideration of a dislocation-dominant mechanism so that the mutual interaction of GNDs at shallow indents plays a critical role in determining this scaling law. Moreover, the proposed law has been verified by comparison with different sets of experimental data.

Author Contributions: Conceptualization, X.X. and L.Y.; writing—original draft preparation, X.X.; writing—review and editing, H.L. and L.Y.; supervision, X.X.; project administration, X.X.; funding acquisition, H.L. and X.X. All authors have read and agreed to the published version of the manuscript.

Funding: This work is supported by the National Nature Science Foundation of China (NSFC) under Contract No. 11802344, 11872379 and 11805061, and the Natural Science Foundation of Hunan Province, China (Grant No. 2019JJ50809 and 2019JJ50072). Hao Liu thanks the Fundamental Research Funds for the Central Universities.

Conflicts of Interest: The funders had no role in the design of the study; in the collection, analyses, or interpretation of data; in the writing of the manuscript, or in the decision to publish the results.

References

1. Maier-Kiener, V.; Durst, K. Advanced Nanoindentation Testing for Studying Strain-Rate Sensitivity and Activation Volume. *JOM* **2017**, *69*, 2246–2255. [CrossRef] [PubMed]
2. Alkorta, J.; Martinez-Esnaola, J.M.; Sevillano, J.G. Critical examination of strain-rate sensitivity measurement by nanoindentation methods: Application to severely deformed niobium. *Acta Mater.* **2008**, *56*, 884–893. [CrossRef]
3. Gibson, J.S.K.L.; Schroeders, S.; Zehnder, C.; Korte-Kerzel, S. On extracting mechanical properties from nanoindentation at temperatures up to 1000 °C. *Extreme Mech. Lett.* **2017**, *17*, 43–49. [CrossRef]
4. Mayo, M.J.; Siegel, R.W.; Narayanasamy, A.; Nix, W.D. Mechanical properties of nanophase TiO_2 as determined by nanoindentation. *J. Mater. Res.* **1990**, *5*, 1073–1082. [CrossRef]
5. Lucas, B.N.; Oliver, W.C. Indentation power-law creep of high-purity indium. *Met. Mater. Trans. A* **1999**, *30*, 601–610. [CrossRef]
6. Mayo, M.; Nix, W. A micro-indentation study of superplasticity in Pb, Sn, and Sn-38 wt% Pb. *Acta Met.* **1988**, *36*, 2183–2192. [CrossRef]
7. Maier, V.; Durst, K.; Mueller, J.; Backes, B.; Hoeppel, H.W.; Goeken, M. Nanoindentation strain-rate jump tests for determining the local strain-rate sensitivity in nanocrystalline Ni and ultrafine-grained Al. *J. Mater. Res.* **2011**, *26*, 1421–1430. [CrossRef]
8. Elmustafa, A.A.; Stone, D.S. Nanoindentation and the indentation size effect: Kinetics of deformation and strain gradient plasticity. *J. Mech. Phys. Solids* **2003**, *51*, 357–381. [CrossRef]
9. Zhao, J.; Wang, F.; Huang, P.; Lu, T.J.; Xu, K.W. Depth dependent strain rate sensitivity and inverse indentation size effect of hardness in body-centered cubic nanocrystalline metals. *Mater. Sci. Eng. A* **2014**, *615*, 87–91. [CrossRef]
10. Niu, J.J.; Zhang, J.Y.; Liu, G.; Zhang, P.; Lei, S.Y.; Zhang, G.J.; Sun, J. Size-dependent deformation mechanisms and strain-rate sensitivity in nanostructured Cu/X (X = Cr, Zr) multilayer films. *Acta Mater.* **2012**, *60*, 3677–3689. [CrossRef]
11. Wei, Q. Strain rate effects in the ultrafine grain and nanocrystalline regimes-influence on some constitutive responses. *J. Mater. Res.* **2007**, *42*, 1709–1727. [CrossRef]
12. Bai, Z.; Fan, Y. Abnormal Strain Rate Sensitivity Driven by a Unit Dislocation-Obstacle Interaction in bcc Fe. *Phys. Rev. Lett.* **2018**, *120*, 125504. [CrossRef] [PubMed]
13. Chen, J.; Lu, L.; Lu, K. Hardness and strain rate sensitivity of nanocrystalline Cu. *Scr. Mater.* **2006**, *54*, 1913–1918. [CrossRef]
14. Nyakiti, L.O.; Jankowski, A.F. Characterization of Strain-Rate Sensitivity and Grain Boundary Structure in Nanocrystalline Gold-Copper Alloys. *Met. Mater. Trans. A* **2010**, *41*, 838–847. [CrossRef]
15. Jia, D.; Ramesh, K.T.; Ma, E. Effects of nanocrystalline and ultrafine grain sizes on constitutive behavior and shear bands in iron. *Acta Mater.* **2003**, *51*, 3495–3509. [CrossRef]
16. Li, S.; Wang, F.; Zhang, L.F.; Huang, P. Indentation depth dependence of nanoscale Al/W multilayers on strain rate sensitivity. *Mater. Sci. Eng. A* **2019**, *767*, 138438. [CrossRef]
17. Bhakhri, V.; Klassen, R.J. The depth dependence of the indentation creep of polycrystalline gold at 300 K. *Scr. Mater.* **2006**, *55*, 395–398. [CrossRef]
18. Klassen, R.J.; Diak, B.J.; Saimoto, S. Origin of the depth dependence of the apparent activation volume in polycrystalline 99.999% Cu determined by displacement rate change micro-indentation. *Mater. Sci. Eng. A* **2004**, *387*, 297–301. [CrossRef]
19. Peykov, D.; Martin, E.; Chromik, R.R.; Gauvin, R.; Trudeau, M. Evaluation of strain rate sensitivity by constant load nanoindentation. *J. Mater. Res.* **2012**, *47*, 7189–7200. [CrossRef]
20. Liu, W.; Wang, Y.; Ma, Y.; Huang, Y.; Tang, Y.; Cheng, F. Indentation size effect of stress exponent and hardness in homogeneous duplex eutectic 80Au/20Sn. *Mater. Lett.* **2014**, *120*, 151–154. [CrossRef]
21. Sadeghilaridjani, M.; Muskeri, S.; Hasannaeimi, V.; Pole, M.; Mukherjee, S.; Hassannaeimi, V. Strain rate sensitivity of a novel refractory high entropy alloy: Intrinsic versus extrinsic effects. *Mater. Sci. Eng. A* **2019**, *766*, 138326. [CrossRef]
22. Li, H.; Ngan, A.H.W. Size effects of nanoindentation creep. *J. Mater. Res.* **2004**, *19*, 513–522. [CrossRef]
23. Haghshenas, M.; Wang, L.; Klassen, R.J. Depth dependence and strain rate sensitivity of indentation stress of 6061 aluminium alloy. *Mater. Sci. Technol.* **2012**, *28*, 1135–1140. [CrossRef]

24. Wei, Q.; Cheng, S.; Ramesh, K.T.; Ma, E. Effect of nanocrystalline and ultrafine grain sizes on the strain rate sensitivity and activation volume: Fcc versus bcc metals. *Mater. Sci. Eng. A* **2004**, *381*, 71–79. [CrossRef]
25. Liu, Y.; Hay, J.; Wang, H.; Zhang, X. A new method for reliable determination of strain-rate sensitivity of low-dimensional metallic materials by using nanoindentation. *Scr. Mater.* **2014**, *77*, 5–8. [CrossRef]
26. Asaro, R.J.; Suresh, S. Mechanistic models for the activation volume and rate sensitivity in metals with nanocrystalline grains and nano-scale twins. *Acta Mater.* **2005**, *53*, 3369–3382. [CrossRef]
27. Lu, L.; Dao, M.; Zhu, T.; Li, J. Size dependence of rate-controlling deformation mechanisms in nanotwinned copper. *Scr. Mater.* **2009**, *60*, 1062–1066. [CrossRef]
28. Cao, Z.H.; Li, P.Y.; Lu, H.M.; Huang, Y.L.; Zhou, Y.C.; Meng, X.K. Indentation size effects on the creep behavior of nanocrystalline tetragonal Ta films. *Scr. Mater.* **2009**, *60*, 415–418. [CrossRef]
29. Cao, Z.H.; Huang, Y.L.; Meng, X.K. Size-dependent rate sensitivity and plasticity of nanocrystalline Ru films. *Scr. Mater.* **2010**, *63*, 993–996. [CrossRef]
30. Mohammed, Y.S.; Stone, D.S.; Elmustafa, A.A. Strain Rate Sensitivity of the Nanoindentation Creep of Ag, Cu, and Ni Thin Films. *JOM* **2019**, *71*, 3734–3743. [CrossRef]
31. Gu, P.; Dao, M.; Asaro, R.J.; Suresh, S. A unified mechanistic model for size-dependent deformation in nanocrystalline and nanotwinned metals. *Acta Mater.* **2011**, *59*, 6861–6868. [CrossRef]
32. Haghshenas, M.; Khalili, A.; Ranganathan, N. On room-temperature nanoindentation response of an Al-Li-Cu alloy. *Mater. Sci. Eng. A* **2016**, *676*, 20–27. [CrossRef]
33. Sadeghilaridjani, M.; Mukherjee, S. High-temperature nano-indentation creep behavior of multi-principal element alloys under static and dynamic loads. *Metals* **2020**, *10*, 250. [CrossRef]
34. Ma, Z.S.; Long, S.G.; Zhou, Y.C.; Pan, Y. Indentation scale dependence of tip-in creep behavior in Ni thin films. *Scr. Mater.* **2008**, *59*, 195–198. [CrossRef]
35. Haghshenas, M.; Klassen, R.J. Assessment of the depth dependence of the indentation stress during constant strain rate nanoindentation of 70/30 brass. *Mater. Sci. Eng. A* **2013**, *572*, 91–97. [CrossRef]
36. Maier, V.; Schunk, C.; Goeken, M.; Durst, K. Microstructure-dependent deformation behaviour of bcc-metals—indentation size effect and strain rate sensitivity. *Philos. Mag.* **2015**, *95*, 1766–1779. [CrossRef]
37. Long, X.; Tang, W.; Feng, Y.; Chang, C.; Keer, L.M.; Yao, Y. Strain rate sensitivity of sintered silver nanoparticles using rate-jump indentation. *Int. J. Mech. Sci.* **2018**, *140*, 60–67. [CrossRef]
38. Kasada, R.; Konishi, S.; Hamaguchi, D.; Ando, M.; Tanigawa, H. Evaluation of strain-rate sensitivity of ion-irradiated austenitic steel using strain-rate jump nanoindentation tests. *Fusion Eng. Des.* **2016**, *109*, 1507–1510. [CrossRef]
39. Liu, Y.; Liu, W.; Yu, L.; Chen, L.; Sui, H.; Duan, H. Hardening and Creep of Ion Irradiated CLAM Steel by Nanoindentation. *Crystals* **2020**, *10*, 44. [CrossRef]
40. Stegall, D.E.; Elmustafa, A.A. The Contribution of Dislocation Density and Velocity to the Strain Rate and Size Effect using Transient Indentation Methods and Activation Volume Analysis. *Met. Mater. Trans. A* **2018**, *49*, 4649–4658. [CrossRef]
41. Nix, W.D.; Gao, H.J. Indentation size effects in crystalline materials: A law for strain gradient plasticity. *J. Mech. Phys. Solids* **1998**, *46*, 411–425. [CrossRef]
42. Kobrinsky, M.J.; Thompson, C.V. Activation volume for inelastic deformation in polycrystalline Ag thin films. *Acta Mater.* **2000**, *48*, 625–633. [CrossRef]
43. Lee, S.; Meza, L.; Greer, J.R. Cryogenic nanoindentation size effect in [001]-oriented face-centered cubic and body-centered cubic single crystals. *Appl. Phys. Lett.* **2013**, *103*, 101906. [CrossRef]
44. Xiao, X.; Chen, Q.; Yang, H.; Duan, H.; Qu, J. A mechanistic model for depth-dependent hardness of ion irradiated metals. *J. Nucl. Mater.* **2017**, *485*, 80–89. [CrossRef]
45. Xiao, X.; Song, D.; Xue, J.; Chu, H.; Duan, H. A self-consistent plasticity theory for modeling the thermo-mechanical properties of irradiated FCC metallic polycrystals. *J. Mech. Phys. Solids* **2015**, *78*, 1–16. [CrossRef]
46. Gurson, A.L. Continuum theory of ductile rupture by void nucleation and growth: Part I—Yield criteria and flow rules for porous ductile media. *J. Eng. Mater. Technol.* **1977**, *99*, 2–15. [CrossRef]
47. Tabor, D. A simple theory of static and dynamic hardness. *Proc. R. Soc. Lond. Ser. A* **1948**, *192*, 247–274.
48. Cheng, Y.T.; Cheng, C.M. Scaling, dimensional analysis, and indentation measurements. *Mater. Sci. Eng. R* **2004**, *44*, 91–149. [CrossRef]

49. Elmustafa, A.A.; Stone, D.S. Size-dependent hardness in annealed and work hardened at-brass and aluminum polycrystalline materials using activation volume analysis. *Mater. Lett.* **2003**, *57*, 1072–1078. [CrossRef]
50. Butt, M.Z.; Feltham, P. Work-hardening of polycrystalline copper and alpha brasses. *Met. Sci.* **1984**, *18*, 123–126. [CrossRef]
51. Lin, M.R.; Wagoner, R.H. Effect of temperature, strain, and strain rate on the tensile flow-stress of I.F. steel and strainless-steel Type-310. *Scr. Met.* **1986**, *20*, 143–148. [CrossRef]
52. Zehetbauer, M.; Seumer, V. Cold work-hardening in stage-IV and stage-V of F.C.C. metals—I. Experiments and indentation. *Acta Met. Mater.* **1993**, *41*, 577–588. [CrossRef]